Advancements in PRISM: DLR processing framework for interferometric SAR missions

Matteo Nannini, André Barros Cardoso da Silva, Andrea Pulella, Gustavo Daniel Martín-del-Campo-Becerra, Nida Sakar, Johannes Kramp, Jun Su Kim, Pau Prats-Iraola
German Aerospace Center (DLR), Microwaves and Radar Institute, Münchener Straße 20 Weßling

Abstract

PRISM (PRocessor for Interferometric SAR Missions) is the new SAR processing framework developed at the Microwaves and Radar institute of the German Aerospace Center (DLR) [1]. This framework allows efficient and accurate processing of SAR data up to interferogram generation. Moreover, the software design has been studied to allow in a flexible way to handle SAR data independently on the sensor and the mode with which they have been acquired. This is paramount in order to process the large variety of data acquired with different sensors and, more important, to tackle challenges that future missions like NISAR (USA/India), BIOMASS (ESA), Harmony (ESA) and ROSE-L (ESA) will present. In this paper, the two main components of PRISM, the focusing and interferometric chain, are recalled along with a description of the processor software architecture. Latest results achieved with simulated ROSE-L data, and ALOS data will be shown.

1 SAR Processor

The main blocks of the phase-preserving SAR processor implemented in PRISM are shown in **Figure 1**. By means of the geometry, the RAW data are processed by undergoing the depicted processing steps. One can observe that PRISM is designed to optionally include the azimuth reconstruction step (a.k.a. as MAPS processing) prior to the data SAR focusing. This step is necessary if high-resolution wide-swath (HRWS) data are acquired from several channels beneath the Nyquist rate and to recover the unaliased spectrum [2][3]. Such technique will be used with the ROSE-L (Radar Observation System for Europe in L-band) mission [4], where five channels in azimuth are acquired, as well as in the future Sentinel-1 NG (Next Generation) mission.

Concerning the image formation steps, range processing can be carried out by exploiting both a nominal chirp or a replica obtained from the internal calibration. The correction of the range cell migration can be carried out by means of algorithms such extended chirp scaling [5] or omega-k [6][7]. Those algorithms can be also employed for the azimuth compression if the acquisition mode is stripmap, but for multi-swath acquisitions, like ScanSAR or TOPS, PRISM flexibility allows to perform such step via the Baseband Azimuth Scaling (BAS) algorithm [8]. It is worth mentioning that the processing includes antenna pattern compensation operations like, for example, Scan-On-Receive (SCORE), as it is the case for ROSE-L [9].

PRISM includes advanced processing algorithms to handle specific aspects, that otherwise would degrade the quality of the processed data, such as the Postprocessing Algorithm for Squint and Topography Accommodation: PASTA [10] and the Ionospheric correction for single image [11]. A brief description of those approaches concludes this section, while results obtained by applying PASTA are reported in Section 4.1.1 for the ROSE-L case.

Once the raw data are processed, a post-processing step is foreseen to generate breakpoint data of the multilooked

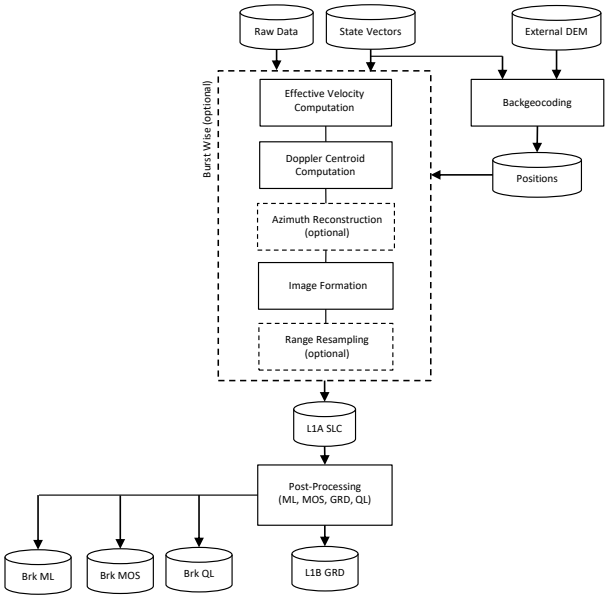

Figure 1 Overview of the focusing PRISM chain.

data (BrK ML), mosaicked data (BrK MOS) as well as the quick look images (BrK QL). Finally, the ground range detected (GRD) data product is obtained (L1B GRD).

1.1 PASTA

This algorithm tackles the problem of inaccurate focusing when the range histories of targets are different with respect to a reference one located at a reference azimuth location. This is necessary especially when increasing the azimuth resolution or the squint angle (as is the case of future missions like ROSE-L), because in such cases, the curvature of the orbit and the rotation of the Earth needs to be accurately accounted for, differently from what it is generally done with the commonly assumed linear-track approximation. PASTA accommodates the different range curva-

ture for the targets located at the same zero-Doppler distance as a function of their altitude and azimuth position. This is done with a block-wise topographic dependent phase correction applied on the already focused data. Section 4.1.1 shows the impact and the need of such correction for future missions like ROSE-L.

1.2 Ionospheric Correction at SLC Level

The ionosphere poses an important challenge to radar signal integrity, potentially leading to data corruption. The severity of this effect hinges on the radar wavelength and acquisition conditions. Fortunately, PRISM offers a solution by estimating and mitigating the Faraday Rotation (FR), group delay, and ionospheric phase.

FR is the alteration of the polarization state of microwave electromagnetic (EM) waves as they traverse the ionosphere's birefringent properties. Mathematically, FR is described as the application of a rotation matrix [R] on both the left and right sides of the scattering matrix [S_0], such that [S]=[R][S_0][R]. This operation is not unitary, causing the loss of reflection symmetry. Thus, the off-diagonal elements of the scattering matrix, which are normally equal due to reciprocity, become distinct. This distinctiveness allows for the estimation of FR from quad-pol SAR data. Matrix [R] is determined by the FR angle Ω, which can be estimated via the Bickel and Bates approach [11].

The ionosphere's dispersive nature results in slower group velocity for EM waves. SAR images, imaged through the ionosphere, may exhibit undesired slant-range displacement. This displacement can be calculated using the Total Electric Content (TEC), derived from the smoothed FR estimate and the parallel geomagnetic field. TEC also aids in computing the ionospheric phase screen, enabling precise correction of the ionospheric phase component in radar signals.

2 InSAR Processor

The interferometric SAR (InSAR) chain consists of the coregistration of two single-look complex (SLC) images forming an interferometric pair, followed by the generation of the interferogram and the reprojection of the interferometric outcomes into a geographic coordinate system based on an external DEM. **Figure 2** reports the main processing blocks for the Interferometric Processor chain implemented in PRISM, with the optional steps marked as dashed blocks. Given a pair of focused SAR products (L1A SLC) with the corresponding annotation parameters, the processing chain requires as auxiliary inputs an external digital elevation model (DEM) and the state vectors (e.g., orbital positions and velocity of the satellite) associated with the chosen reference orbit. Thanks to its versatile block structure, PRISM is able to retrieve the InSAR results regardless of the acquisition mode (StripMap, ScanSAR, TOPS) and to activate/deactivate blocks of the chain according to the configuration settings defined by the user. In the Backgeocoding block, the azimuth and range positions of each acquisition are measured and used to calculate

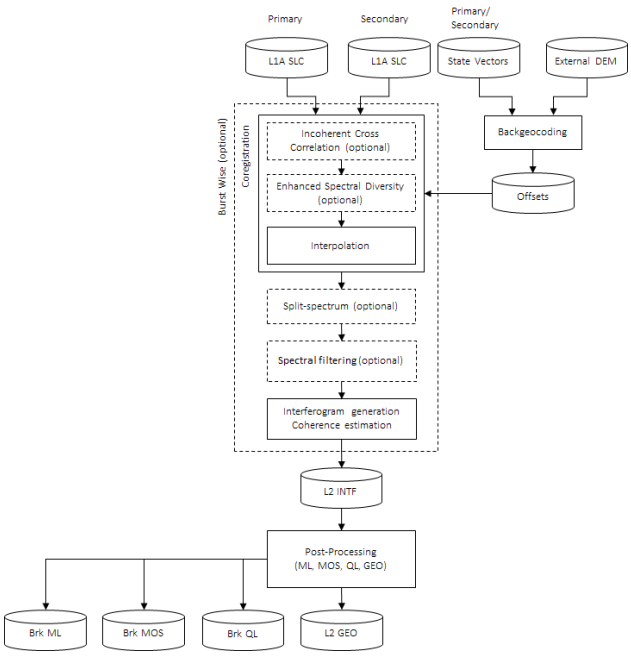

Figure 2 Overview of the InSAR PRISM chain.

the offsets between the secondary and primary acquisitions. Without changing the main architecture, PRISM allows the user to select a desired external DEM (e.g. SRTM at 90 m, Copernicus DEM at 30 m). Given the pre-computed offset matrices, the Coregistration block handles the resampling of the secondary acquisition in the slant-range grid of the primary image. PRISM provides the ability to apply various refinements to the offsets to improve the accuracy of the coregistration. Different state-of-the-art methods are included in PRISM, such as Enhanced Spectral Diversity (ESD) [12] for the multi-swath modes and Incoherent Cross-Correlation (ICC) [13]. After the Coregistration step, the user can choose to execute the Split-spectrum block to compensate for ionospheric effects in interferograms using the methods described in [14],[15]. When the Spectral filtering block is activated, PRISM can also mitigate the spectral decorrelation caused by the different acquisition geometries. Therefore, in the Interferogram generation block, PRISM allows the usage of a set of different state-of-the-art filters for interferogram computation and coherence estimation. Similar to the SAR Processor, the post-processing step generates different breakpoint/output data from the interferometric results (L2 INTF):

1. BrK ML: spatial multi-looking (ML) filtering is applied using configurable output resolutions on ground (which define the bandwidths along range and azimuth) and configurable weighting windows;
2. BrK MOS: in the case of burst mode, de-bursting and subswaths merging are applied to provide a mosaicked product;
3. BrK QL: quick look images are stored for visual inspection.

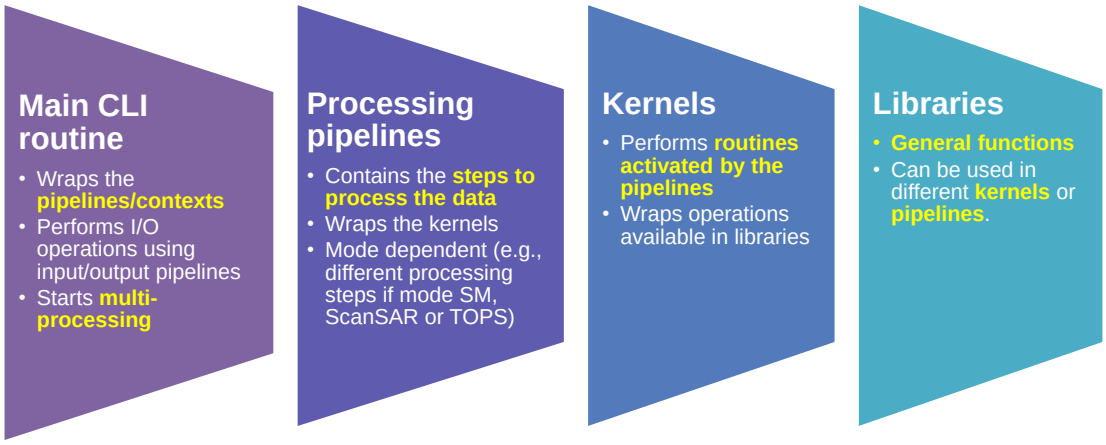

Figure 3 Main blocks of PRISM architecture.

4. L2-GEO: accurate geocoding is applied using as reference the user-defined external DEM applied in the Backgeocoding block;

Among the blocks depicted in **Figure 2**, some implementation details on the split-spectrum technique are reported in the following dedicated subsection.

2.1.1 Estimation of the ionospheric phase screen: split-spectrum method

The most accurate way of absolute (i.e. single-image) TEC estimation is described in Section 1.2, exploiting the FR. However, FR-derived TEC estimates might not be sensitive enough in some cases for for interferometric applications, since the performance of this technique depends strongly on the latitude, less sensitive close to the geomagnetic equator. By instance, at L-band one TECU (=1016 electrons per m^2) of ionosphere leads to 13.6 radians of phase advance. Therefore, in interferometric applications, any spatial or temporal TEC variation between two acquisitions is corrupting the interferometric phase. The split-spectrum approach [14] is the most accurate and robust way for isolating and estimating the ionospheric phase contribution (i.e. the ionospheric phase screen) from the topographic and tropospheric contributions in SAR interferograms.

Due to the dispersive nature of the ionosphere, the interferometric phase pattern varies with changing frequency. The ionospheric phase screen $\Delta\phi_{iono}$ is calculated by the weighted difference ($\Delta\phi = \Delta\phi_H - \Delta\phi_L$) and sum ($\Sigma\phi = \Delta\phi_H + \Delta\phi_L$) of the interferometric phases at higher and lower frequency bands ($\Delta\phi_H$ and $\Delta\phi_L$, respectively):

$$\Delta\Phi_{iono} = -f_0\Delta\Phi/(4\Delta f) + \Sigma\phi/4 \qquad (1)$$

where f_0 is the center frequency and Δf is the spectral separation between the lower or the higher frequency sub-band and f_0. Once can observe that, since the upscaling factor $f_0/4\Delta f$ is quite large (but still smaller than the FR to phase scaling factor), a strong spatial averaging is required for a robust implementation of the so-called split-bandwidth method. As a result, small scale ionospheric features may remain after correction using the split-spectrum method. Results obtained by applying such method are reported in Section 4.1.2, using stripmap L-band ALOS data acquired over northern Alaska.

3 PRISM Architecture

The software architecture of PRISM has been designed to allow mode- and format-independent processing of SAR data in a flexible and accurate manner. A key point is the modular structure of PRISM, that allows this framework to be easy upgradable in order to meet the needs of future SAR missions that will be implemented with new technologies and techniques. In addition, PRISM makes available to the user a wide spectrum of state-of-the-art techniques that can be easily selected via a processing configuration file.

Figure 3 shows the main blocks of the architecture of PRISM. Analysing the chart from left to right, one can observe that PRISM is an ensemble of components operating and being activated at different levels. The main PRISM calls are orchestrated by command line interface (CLI) routine that will define the necessary processing, the proper I/O pipelines and start the processing itself. Then, the started pipeline will handle the higher-level flow necessary for the processing and, depending on the mode, the correct kernels will be activated. The kernels do represent the key functionalities on which PRISM is built. Selected kernels are activated and executed depending on the defined pipeline, including, for example, the proper processing steps (e.g. ECS, BAS), coregistration algorithms (e.g. ESD) and additional correction algorithms (e.g. PASTA, ionospheric correction). Apart from kernels inherent functionalities, more generic ones are implemented in independent libraries, such that they are available also at higher level pipelines or for other kernels.

PRISM framework is python-based, but it has the flexibility to execute both native Python libraries as well as third-party ones in order to improve efficiency. PRISM offers in addition the possibility to use both multiprocessing and multithreading simultaneously, depending on the user needs and the target machine. Due to the increasing data

dimension that characterizes modern SAR systems, efficiency becomes more and more a key parameter also for experimental frameworks like PRISM. Due to its flexible and modular structure, an extension of PRISM to exploit cloud computing will be addressed in the near future.

4 Case studies

In this section new results obtained with the PRISM framework are presented. Firstly, in Section 4.1.1, the impact of the correction for the space variance of the effective velocity by means of the PASTA algorithm will be shown. In particular, the processed data consist of a scene simulating an acquisition in the frame of the ROSE-L mission. The RAW data have been simulated by DLR's end-to-end tool [16]. Secondly, in Section 4.1.2, ALOS data acquired over Alaska are processed to extract the ionospheric phase screen with the interferometric split-spectrum technique.

4.1.1 PASTA results

A first test on PASTA has been carried out on a ROSE-L-like data set simulated at a 0m height. PRISM processed the data and generated both the focused data before applying PASTA and after such correction is applied. By means of azimuth phase profiles one can observe the impact of the correction of PASTA, which are shown in **Figure 4** for a point target processed with a height bias of 1000m. **Figure 4(top)** shows the phase error before applying PASTA, which clearly presents a quadratic phase error due to the mismatch between the processing and target's height, i.e., a mis-match in the Doppler rate. This plot shows only the quadratic component, but note that a linear term is also present, hence resulting in an azimuth geolocation error of 90 centimeters. Results after applying PASTA post-processing are shown in **Figure 4(bottom)**, where note that the bias has been corrected on the final focused image after properly considering the right topography of the target. In addition, the geolocation accuracy in azimuth is now right.

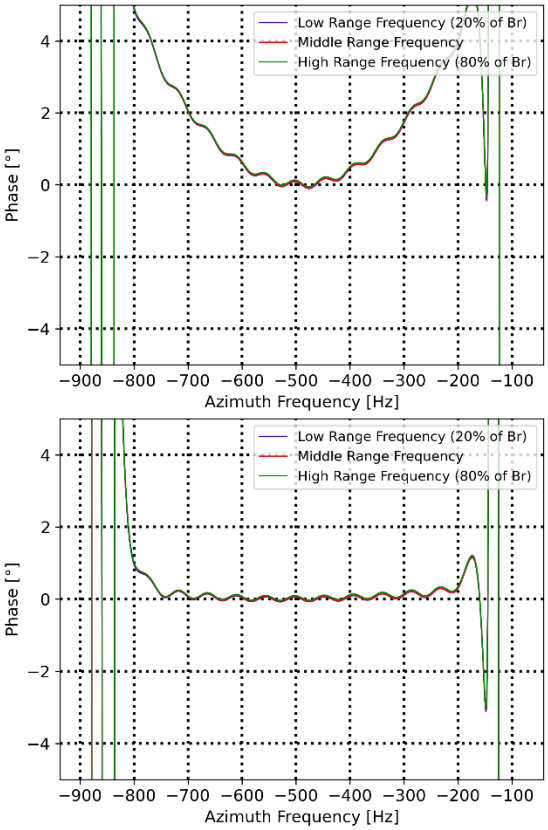

Figure 4 Azimuth phase profile of a target processed with (top) topographic height of 1000m and (bottom) with post-processing PASTA method accounting for the reference height bias.

4.1.2 Ionospheric mitigation results

Aimed at assessing practicality, the split-spectrum method has been applied using stripmap L-band ALOS data (HH polarization) acquired in northern Alaska during the months of April and May in 2007. The geographical extent of the dataset is represented in **Figure 5**. The corresponding interferogram, depicted in **Figure 6(a)**, shows phase changes due to the spatial variations in the ionospheric TEC. By instance, several fringes due to ionospheric variations can be seen in the bottom half of the interferogram. After the calculation of interferograms at each lower and higher sub-band, the topographic phase was removed using a DEM. Since the coherence is sufficiently high, as shown in **Figure 6(b)**, phase unwrapping was carried out without any issues. The ionosphere typically presents relatively smooth patterns and its estimates are often spatially correlated. Therefore, a 2D Gaussian weighted filter [14] is utilized to smooth the recovered ionospheric phase and remove high-frequency noise components. The weighting was determined by approximating the interferometric

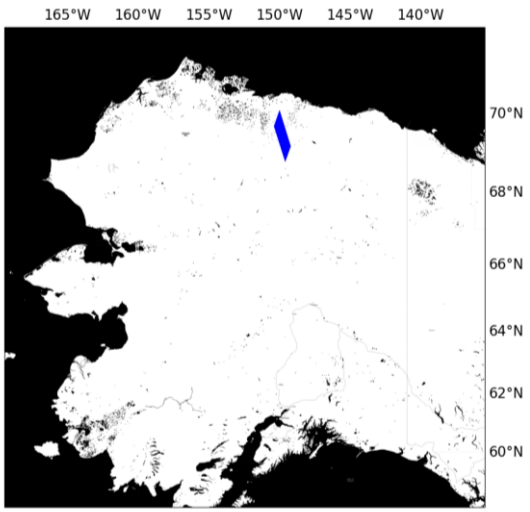

Figure 5 Ground coverage (blue) of ALOS acquisitions in northern Alaska.

phase variance of the two sub-bands. The output of the split-spectrum method is then transformed into a phase screen [**Figure 6(c)**], which is posteriorly used to correct the original interferogram. Although the accuracy of the split-spectrum method is constrained by a narrow range bandwidth of 14 MHz, **Figure 6(d)** depicts the successful

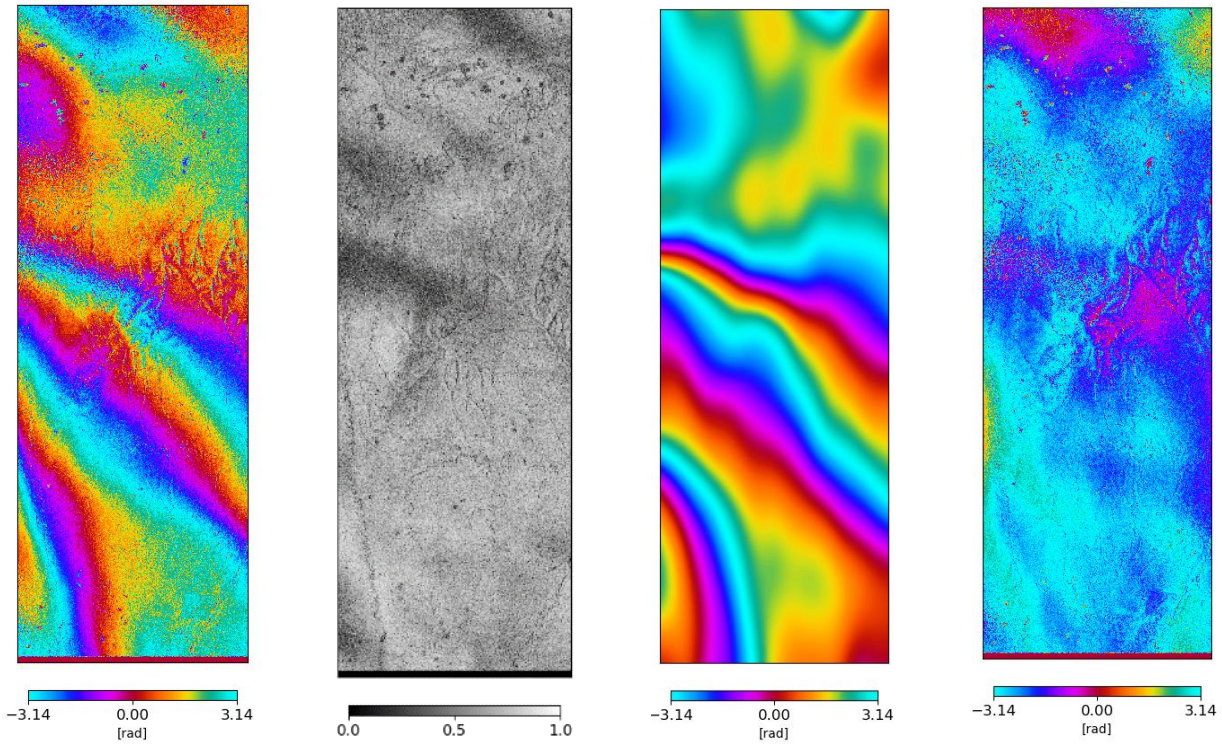

Figure 6 Ionospheric estimation: (a) Spatial variations in the ionospheric TEC mapped as phase changes in the interferogram. (b) Interferometric coherence. (c) Ionospheric phase screen estimated using the split-spectrum method. (d) Ionosphere-compensated interferogram.

removal of most ionospheric contributions. Currently, the split-bandwidth method is being extended in PRISM to handle multi-swath modes, as expounded in [15].

5 Conclusions

In this contribution, the status of the PRISM processing framework, currently being developed at the Microwaves and Radar Institute of DLR, has being presented. The primary goal of this framework is to allow the processing of SAR data from raw data up to interferogram level. This is achieved thanks to a software architecture design allowing for a format-, sensor- and mode-independent processing. This is fundamental to meet future and present needs, since the variety of SAR missions is increasing along with their complexity and the data dimensions. In such sense, particularly important are the multiprocessing and multithreading capabilities of the framework, which are being implemented in order to ease the extension of PRISM to cloud computing environments. With PRISM it is possible to exploit the potentiality of state-of-the-art techniques for SAR missions due to its easy upgradable structure. In this sense, results concerning the space variance correction carried out with the PASTA technique and the ionospheric phase screen estimation via split-bandwidth have been presented in Sections 4.1.1 and 4.1.2, showing the reliability of the processor.

Future upgrades will include the antenna pattern compensation for SCORE systems, as well as the extension of split-bandwidth to multi-swath acquisitions.

6 Literature

[1] Nannini, M., Barros Cardoso Da Silva, A., Pulella, A., Sakar, N., Kramp, J., Martín-del-Campo-Becerra, G. D., ... & Prats-Iraola, P. (2023, May). PRISM: A Flexible Experimental Processing Framework For Present And Future SAR Missions. In 2023 24th International Radar Symposium (IRS) (pp. 1-10). IEEE.

[2] G. Krieger, N. Gebert, A. Moreira: Unambiguous SAR Signal Reconstruction from Nonuniform Displaced Phase Center Sampling, in IEEE Geoscience and Remote Sensing Letters, vol. 1, no. 4 (2004): 260-264.

[3] N. Gebert, G. Krieger, and A. Moreira: Digital beamforming on receive: Techniques and optimization strategies for highresolution wide-swath SAR imaging, IEEE Trans. Aerosp. Electron. Syst., vol. 45 (2009): 564–592.

[4] ROSE-L Mission Requirement Document (MRD), ESA-EOPSM-CLIS-MRD-3371, issue 2.0

[5] A. Moreira, J. Mittermayer, and R. Scheiber: Extended Chirp Scaling Algorithm for Air- and Spaceborne SAR Data Processing in Stripmap and ScanSAR Imaging Modes IEEE Transactions on Geoscience and Remote Sensing, vol. 34, no. 5 (1996): 1123-1136.

[6] I. A. Cumming, and F. H. Wong: Digital Processing of Synthetic Aperture Radar Data. Boston, MA: Artech House, 2004.

[7] R. H. Stolt: Migration by transform. Geophysics, vol. 43, no. 1 (1978): 23-48.

[8] P. Prats, R. Scheiber, J. Mittermayer, A. Meta, and A. Moreira: Processing of Sliding-Spotlight and TOPS SAR Data Using Baseband Azimuth Scaling, IEEE Transactions on Geoscience and Remote Sensing, vol. 48, no. 2 (2010): 770-780.

[9] M. Suess, B. Grafmueller, R. Zahn: A novel high resolution, wide swath SAR system, in Proc. IGARSS, Sydney, Australia, 2001.

[10] M. Rodriguez-Cassola, P. Prats-Iraola, F. De Zan, R. Scheiber, A. Reigber, D. Geudtner, A. Moreira: Doppler-related distortions in TOPS SAR images, IEEE TGRS, 2015.

[11] J. S. Kim, K. Papathanassiou, R. Scheiber and S. Quegan: Correcting distortion of polarimetric SAR data induced by ionospheric scintillation, IEEE Transactions on Geoscience and Remote Sensing, vol. 53, no. 12 (2015): 6319-6335.

[12] P. Prats-Iraola, R. Scheiber, L. Marotti, S. Wollstadt, and A. Reigber: TOPS interferometry with TerraSAR-X, IEEE Transactions on Geoscience and Remote Sensing, vol. 50, no. 8 (2012): 3179-3188.

[13] N. Yagüe-Martínez, P. Prats-Iraola, F. R. Gonzalez, R. Brcic, R. Shau, D. Geutner, M. Eineder, and R. Bamler: Interferometric Processing of Sentinel-1 TOPS Data, IEEE Transactions on Geoscience and Remote Sensing, vol. 54, no. 4 (2016): 2220-2234

[14] G. Gomba, A. Parizzi, F. De Zan, M. Eineder and R. Bamler: Toward Operational Compensation of Ionospheric Effects in SAR Interferograms: The Split-Spectrum Method, IEEE Transactions on Geoscience and Remote Sensing, vol. 54, no. 3 (2016): 1446-1461.

[15] G. Gomba, F. R. González, F. De Zan: Ionospheric phase screen compensation for the Sentinel-1 TOPS and ALOS-2 ScanSAR modes, IEEE Transactions on Geoscience and Remote Sensing, vol. 55, no. 1 (2017): 223-235.

[16] V. Queiroz de Almeida, et al.: ROSE-L: Overview and Preliminary Results of the Mission End-To-End Simulator and Ground Prototype Processor, ESA Advanced RF Sensors and Remote Sensing Instruments (ARSI) and ESA Ka-Band Earth Observation Radar Missions (KEO), 2022-05-10 - 2022-05-12, Noordwijk, The Netherlands.